

Mixed Neural Voxels for Fast Multi-view Video Synthesis

Feng Wang¹ Sinan Tan¹ Xinghang Li¹ Zeyue Tian² Huaping Liu¹ *

¹Beijing National Research Center for Information Science and Technology(BNRist),
Department of Computer Science and Technology, Tsinghua University

²Hong Kong University of Science and Technology

wang-f20@mails.tsinghua.edu.cn, hpliu@tsinghua.edu.cn



Figure 1. MixVoxels can quickly reconstruct 4D dynamic scenes, and synthesize novel views in both space and time. After 15 minutes of training for 300-frame scenes, we visualize some frames of the rendered novel view videos. We also visualize the learned scene geometry at the rightmost image. We recommend readers to see the whole videos at <https://fengres.github.io/mixvoxels>.

Abstract

Synthesizing high-fidelity videos from real-world multi-view input is challenging because of the complexities of real-world environments and highly dynamic motions. Previous works based on neural radiance fields have demonstrated high-quality reconstructions of dynamic scenes. However, training such models on real-world scenes is time-consuming, usually taking days or weeks. In this paper, we present a novel method named MixVoxels to better represent the dynamic scenes with fast training speed and competitive rendering qualities. The proposed MixVoxels represents the 4D dynamic scenes as a mixture of static and dynamic voxels and processes them with different networks. In this way, the computation of the required modalities for static voxels can be processed by a lightweight model, which essentially reduces the amount of computation, especially for many daily dynamic scenes dominated by the static background. To separate the two kinds of voxels, we propose a novel variation field to estimate the temporal variance of each voxel. For the dynamic voxels, we design an inner-product time query method to efficiently query multiple time steps, which is essential to

recover the high-dynamic motions. As a result, with 15 minutes of training for dynamic scenes with inputs of 300-frame videos, MixVoxels achieves better PSNR than previous methods. Codes and trained models are available at <https://github.com/fengres/mixvoxels>.

1. Introduction

Dynamic scene reconstruction from multi-view videos is a critical and challenging problem, with many potential applications such as interactively free-viewpoint control for movies, cinematic effects like freeze-frame *bullet time*, novel view replays for sporting events, and various potential VR/AR applications. Recently, neural radiance fields [24] have demonstrated the possibility of rendering photo-realistic novel views for static scenes, with physically motivated 3D density and radiance modelling. Many methods [8, 10, 16, 17, 26, 27, 29, 43, 48] extend the neural radiance fields to dynamic scenes with additional time queries or an explicit deformation field. Many of these methods focus on the monocular input video setting on relatively simple dynamic scenes. To model more complex real-world dynamic scenes, a more practical solution is to use multi-view synchronized videos to provide dense spatial-temporal supervi-

*Corresponding author.

sions [2, 16, 20, 54].

Recently, Li et al. [16] propose a real-world dynamic scene dataset including many challenging situations such as objects of high specularly, topology changes, and volumetric effects. They address the problem by a hierarchical training scheme and the ray importance sampling strategies. Although significant improvements have been achieved, some challenges still exist: (1) The training and rendering take a lot of time and computation resources. (2) Highly dynamic scenes with complex motions are still difficult to track.

In this paper, we focus on the multi-view 3D video synthesis problem and design a novel method named MixVoxels to address the above two challenges. The proposed MixVoxels is based on the explicit voxel-grid representation, which is recently popular due to the fast training and rendering speed on static scenes [6, 25, 39, 49]. We extend the voxel-grid representations to support dynamic scenes and design an efficient inner-product time query to simultaneously query a large number of time steps, which is essential to recover the sharp details for highly-dynamic objects (like a fast-moving hand). Besides, we represent the dynamic scenes as a mixed static-dynamic voxel-grid representation. Specifically, the 3D spaces are split into static and dynamic voxels by our proposed variation field. The two components are processed by different models to reduce the redundant computations for the static space. Theoretically, once a dynamic scene consists of some static spaces, the training speed will benefit from the proposed mixed voxels. For a variety of events that occur in the physical world, the static components of environments are dominated in most cases, and the mixed voxels will speed up the training significantly in these scenarios. Besides, the separation of voxels makes the time-variant model focus on the dynamic regions, avoiding the time-aware voxels being biased by the static spaces and generating blurred motions. We empirically validate it and find that the separation indeed makes the model learn sharp and distinct boundaries for highly-dynamic regions. This also frees our method from the complex importance sampling strategies. With these designs, our method can reconstruct a 300-frame dynamic scene within 15 minutes, using one RTX 3090 GPU. In summary, the contributions are as follows:

- We design a simple yet effective dynamic voxel-grid representation with inner-product time query that efficiently queries many different time steps, improving the rendering qualities for highly dynamic objects.
- We design an efficient variation field to separate static and dynamic spaces and present a mixed voxel-grid representation to accelerate training and rendering.
- We conduct qualitative and quantitative experiments to evaluate our method. As a result, the proposed

MixVoxels achieves competitive or better rendering qualities with a $5000\times$ training speedup compared to implicit dynamic scene representations.

2. Related Works

Novel View Synthesis for Static Scenes: Synthesizing novel views for static scenes is a classical and well-studied problem. Different approaches represent the underlying geometric with different representations. Mesh-based methods [5, 7, 32, 42, 45, 47] represent the scenes with surfaces which is compact and easy to render, while optimizing a mesh to fit complex scenes is challenging. Volume-based methods such as voxel-grid [14, 20, 28, 34, 35] and multi-plane images (MPIs) [9, 23, 37, 38, 44, 53] are more suitable to model the complex and translucent scenes such as smooth and fluid. Particularly, Neural radiance fields [24] represent the scenes with an implicit volumetric neural representation, which employs a coordinate-based neural network to query the density and color for each point. The achieved photo-realistic rendering quality of NeRF led to an explosion of developments in the field. Advances have been made including improving the rendering qualities [3, 41], adapting to more general scenarios [4, 21, 40, 51], accelerating rendering or training speed [6, 19, 39, 49, 50], etc.

Novel View Synthesis for Dynamic Scenes: Synthesizing novel views for dynamic scenes is a more challenging and applicable problem. Recently, many extensions of NeRF for non-rigid dynamic scenes were proposed, which take a monocular video as input to learn the deformation and radiance fields. These methods can be categorized to modelling deformation implicitly [8, 10, 17, 48] (learn the non-decoupled deformation and appearance jointly) and explicitly [26, 27, 29, 43] (learn separated deformation and radiance fields and the deformation fields are usually in the form of relative motion with a canonical static space). Though improvements are achieved, reconstructing the complex general scenes is still difficult with only monocular videos. Most methods are constrained to fixed scenes like human-model or restricted motions. For real-world complex scenes, reconstructing from synchronized multi-view videos is more promising due to the dense supervision for every viewpoint and time instant. Earlier works [11, 54] explore the problem and show the possibility of rendering novel videos from a set of input views. Neural Volumes [20] proposes to use volumetric representations. They employ an encoder-decoder network to convert input images into a 3D volume, and decode the latent representations by the differentiable ray marching operation. [2] presents a data-driven approach for 4D space-time visualization of dynamic scenes by splitting static and dynamic components and using a U-Net structure in screen space to convert intermediate representation to image. Different with this method, our method split the static and dynamic components in the

3D voxel space instead of the pixel space. More recently, DyNerf [16] uses a temporal-aware neural radiance field to address the problem, and proposes some sampling strategies to train it efficiently. Compared with previous methods, they propose a more complicated real-world dataset and validate their method. For accelerating the reconstruction of dynamic scenes, FourierPlenotree [46] proposes to model the dynamics in frequency domain, and generate a Plenotree through multi-view blending to accelerate rendering. They focus on the foreground moving objects extracted via chroma key segmentation, which requires the background should be a pure color (or rely on segmentation algorithms). Concurrent work [15] proposes to accelerate the training of dynamic scenes by modeling the differences of adjacent frames. [36] decomposes the dynamic scenes into static, new and deforming components. Each query is required to forward through all the three branches to determine the probabilities belong to each component. Different with [36], we separate the space voxels through the proposed variation field and only the dynamic queries are required to forward through the dynamic branch, which largely speeds up the training.

Acceleration of Neural Radiance Fields: While Neural radiance fields can render novel views with high fidelity, training and rendering require querying a deep MLP millions of times which is computationally intensive. Many recent methods propose to accelerate the training and rendering speed of NeRF. For rendering, Neural Sparse Voxel Fields [19] proposes a voxel-grid representation to skip over many empty regions. PlenOctree [50] accelerates the rendering process by pre-tabulating the NeRF into a PlenOctree and using the spherical harmonic representation of radiance. Derf [30] and Kilonerf [31] propose to accelerate the rendering speed by dividing the scenes into multiple areas, and employ multiple small network in each area. AutoInt [18] proposes to restructure the MLP network to accelerate the computations of ray integrals, which helps accelerate the rendering speed. For accelerating the training of NeRF, some methods use explicit voxel-grid representations [39, 49] to accelerate the training process and convergence speed. Instant-NGP [25] proposes a multi-resolution hash table structure to accelerate the training. The model sizes of most fast training methods are relatively large due to a large number of voxels. TensoRF [6] proposes to reduce the model size by factorizing the 4D scene tensor into multiple compact low-rank tensor components.

3. Method

In this section, we introduce the proposed MixVoxels, which represents the 4D dynamic scenes as mixtures of static and dynamic voxels. In the following subsections, we will first introduce the voxel-grid representations for static

scenes and our extension to dynamic scenes. Then we introduce the variation field for identifying the dynamic voxels. At last, we introduce how to combine these components into a unified method and provide the implementation details.

3.1. Static Voxel-grid Representation

Neural radiance fields [24] have demonstrated photo-realistic novel viewpoint synthesis, while the training of NeRF requires extensive computation due to millions of neural network queries. For accelerating NeRF, many recent works [6, 19, 39, 49] have explored the explicit volumetric representation, which avoids the huge amount of computation of querying neural network. Specifically, a 3D scene is split into $N_x \times N_y \times N_z$ voxels. The densities and color features are stored in these voxels and denoted as $\mathcal{S}^\sigma \in \mathbb{R}^{N_x \times N_y \times N_z}$ and $\mathcal{S}^c \in \mathbb{R}^{N_x \times N_y \times N_z \times C}$. $\mathcal{S}_{i,j,k}^\sigma$ and $\mathcal{S}_{i,j,k}^c$ represent the learnable density and color feature of the voxel corner at a discrete position (i, j, k) . For a continuous position (x, y, z) , the representation $\mathcal{S}_{x,y,z}$ can be calculated by interpolating the nearest 8 discrete positions. A small MLP network \mathcal{C}_θ is used to parse the color features into RGB values, taking \mathcal{S}^c and view direction \mathbf{d} as input. Formally, the density $\bar{\sigma}$ and color \bar{c} is formulated as:

$$\bar{\sigma}(x, y, z) = \mathcal{S}_{x,y,z}^\sigma, \quad \bar{c}(x, y, z, \mathbf{d}) = \mathcal{C}_\theta(\mathcal{S}_{x,y,z}^c, \mathbf{d}) \quad (1)$$

3.2. Dynamic Voxel-grid Representation

For dynamic scenes, a direct extension is to add the time dimension to the static voxel-grid representation \mathcal{S} explicitly. However, this direct extension is almost memory-prohibitive due to the large and linearly increasing memory footprint. For a 300-frame video, the learned models will occupy 30 GB of memory and be difficult to train with GPUs due to the limitation of GPU memory. To address this problem, we propose a spatially explicit and temporally implicit representation to reduce the memory footprint. Specifically, we represent the dynamic scene as a 4D learnable voxel-grid $\mathcal{G}^\sigma \in \mathbb{R}^{N_x \times N_y \times N_z \times C_1}$ and $\mathcal{G}^c \in \mathbb{R}^{N_x \times N_y \times N_z \times C_2}$. Different from the static scene representations, the densities and colors for all time steps are implicitly encoded as compact features stored in each voxel corner. The compact features will be processed by a time-aware projection to acquire density and color for each time step. Concretely, for the compact sigma feature $\mathcal{G}_{x,y,z}^\sigma$ and color feature $\mathcal{G}_{x,y,z}^c$ in any position (x, y, z) , we employ two MLPs $\mathcal{T}_{\theta_1}^\sigma$ and $\mathcal{T}_{\theta_2}^c$ to increase the feature dimensions for better parsing time-variant density and color. The MLPs here can be viewed as decompressors, decompressing the compact low-dimensional voxel-grid features into more tractable ones. Compared with directly storing high-dimensional features in each voxel, the temporally implicit representation reduces the memory footprint significantly since the shared MLPs only increase memory slightly.

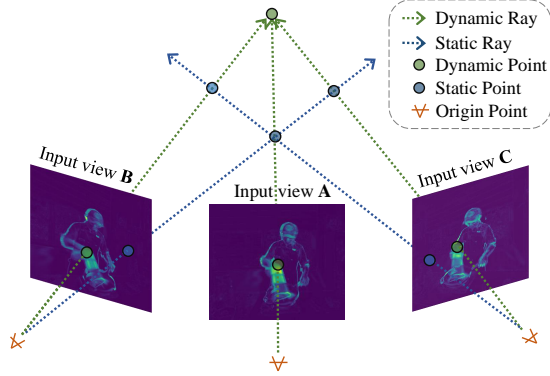


Figure 2. Implicit interaction of multiple rays to decide which point is dynamic. For a static ray (blue line), all points are static. For a dynamic ray (green line), at least one point is dynamic. The intersection of multiple dynamic ray is more likely to be a dynamic point, which is also physically intuitive.

Inner-product time query: For a discrete time step t , we use a learnable time-variant latent representation ω_t to represent the time query. Instead of concatenating the time query with the intermediate features, we propose to calculate the inner product between the learned time query and the decompressed features as the required output σ and c . Formally, the density and color of a space-time query (x, y, z, t) are formulated as:

$$\sigma(x, y, z, t) = \omega_t^\sigma \cdot \mathcal{T}_{\theta_1}^\sigma(\mathcal{G}_{x,y,z}^\sigma) \quad (2)$$

$$c(x, y, z, \mathbf{d}, t) = \omega_t^c \cdot \mathcal{T}_{\theta_2}^c(\mathcal{G}_{x,y,z}^c, \mathbf{d}) \quad (3)$$

In practice, simultaneously querying multiple time steps helps reconstruct the detail of high-dynamic motions and reduces the training iterations to traverse through all time steps. The inner-product based query will facilitate the training speed when simultaneously querying many time steps in a training iteration. Specifically, we denote the FLOPs of the MLP \mathcal{T}_{θ_1} and the inner-product operation as FLOP_{mlp} and FLOP_{inn} , respectively. For a N_t -frame video, the FLOPs of the concatenation query [16] is larger than $N_t \cdot \text{FLOP}_{mlp}$ (due to the extra temporal embedding dimension), while the FLOPs of our inner-product query is only $\text{FLOP}_{mlp} + N_t \cdot \text{FLOP}_{inn}$ ($\text{FLOP}_{mlp} \gg \text{FLOP}_{inn}$).

3.3. Variation Field

In this subsection, we introduce the variation field to identify which voxels in the 3D space are dynamic, i.e., the densities or colors are not constant over different time steps. By separating the static and dynamic voxels, the redundant computations caused by using a relatively heavy time-varying model to process the static components will be avoided, which accelerates the training and rendering.

The core of the variation field is to use the pixel-level temporal variances of multi-view videos as the supervision to estimate the voxel-level variances. The pixel-level (or

ray-level) temporal variances of different videos are shown in Fig 2. Formally, given a ray $\mathbf{r}(s) = \mathbf{o} + s \cdot \mathbf{d}$ with origin \mathbf{o} and direction \mathbf{d} , the corresponding pixel color at time step t is defined as $C^{(t)}(\mathbf{r})$. Then the pixel-level temporal variance $D^2(\mathbf{r})$ is formalized as:

$$D^2(\mathbf{r}) = \frac{1}{N_t} \sum_{t=1}^{N_t} (C^{(t)}(\mathbf{r}) - \bar{C}(\mathbf{r}))^2, \quad \bar{C}(\mathbf{r}) = \frac{1}{N_t} \sum_{t=1}^{N_t} C^{(t)}(\mathbf{r})$$

where $\bar{C}(\mathbf{r})$ is the mean color of pixel corresponding to the ray \mathbf{r} . Note that the variance here is a biased form without Bessel's correction. We find no obvious difference in our method between the two variance estimations. For identifying the dynamic pixels, the standard deviation $D(\mathbf{r})$ is binarized to $M(\mathbf{r})$ with a threshold γ to provide pixel-level dynamic supervision, i.e. $M(\mathbf{r}) = 1$ if $D(\mathbf{r}) \geq \gamma$, else $M(\mathbf{r}) = 0$. In this way, we judge that a ray \mathbf{r} is dynamic if $M(\mathbf{r}) = 1$. Next, we use the $M(\mathbf{r})$ as supervision to estimate the voxel-level variations \mathcal{V} .

The relations between the pixel-level variance and voxel-level variance lie in the following aspects: (1) If a pixel is static, then all voxels passed through by the ray corresponding to the pixel should be static. (2) If a pixel is dynamic, then at least one of the voxels passed through by the corresponding ray is dynamic. Fig 2 shows the two situations. With the above two relations, we design the variation field, which is denoted as $\mathcal{V} \in \mathbb{R}^{N_x \times N_y \times N_z}$ to represent the voxel-level temporal variance. Specifically, we uniformly sample N_s points from the near plane to the far plane in \mathbf{r} , and build the following equation to satisfy the two relations mentioned above:

$$\hat{M}(\mathbf{r}) = \text{sigmoid}(\max(\{\mathcal{V}_{\mathbf{r}(s_i)} | i \in \{1, \dots, N_s\}\})) \quad (4)$$

where $\hat{M}(\mathbf{r})$ is an estimation of $M(\mathbf{r})$. Then we train the variation field by the binary cross-entropy loss:

$$\begin{aligned} \underset{\mathcal{V}}{\text{minimize}} \quad \mathcal{L}_v(\mathbf{r}) = \frac{1}{|\mathcal{R}|} \sum_{\mathbf{r}} & -M(\mathbf{r}) \cdot \log(\hat{M}(\mathbf{r})) \\ & - (1 - M(\mathbf{r})) \log(1 - \hat{M}(\mathbf{r})) \end{aligned} \quad (5)$$

By optimizing the above loss function, we can get the learned variation field \mathcal{V} . The training of the variation field is very efficient, usually taking **less than 30 seconds**.

Analysis: The maximization operation well formulates the relations between a pixel and its corresponding voxels. If a pixel is static, then the equations of 4 and 5 will force all voxels passed through by the corresponding ray to be static ($\mathcal{V}_{x,y,z} = 0$). If a pixel is dynamic, Eq 4 requires at least one of the corresponding voxels (i.e., the max value of the voxel variances) to be dynamic ($\mathcal{V}_{x,y,z} = +\infty$). Although we provide no information about which specific voxels in a dynamic ray are dynamic, the implicit interaction of multiple different rays will force the solution to be physically

reasonable. To explain this, we focus on the observable voxels which at least passed through by one ray. If a point (x, y, z) is passed through by at least one static ray, then $\mathcal{V}_{x,y,z}$ will be optimized to 0. If a point (x, y, z) is only passed through by dynamic rays, and not occluded by other dynamic voxels, then $\mathcal{V}_{x,y,z}$ will be optimized to $+\infty$. This is because without occlusion, the above point of (x, y, z) along the dynamic rays will be passed by other static rays (the front space along these rays are observable from other views). We illustrate this situation in Fig 2.

Inference: After the training process, the temporal variation at a specific 3D position (x, y, z) is $\mathcal{V}_{x,y,z}$, which is easily acquired by interpolating the discrete variation field. We then identify a voxel in the scene as dynamic if $\mathcal{V}_{x,y,z}$ is larger than a hyper-parameter β , and as static if it is smaller than β . Formally, we will get a dynamic mask $\bar{\mathbf{M}} \in \{0, 1\}^{N_x \times N_y \times N_z}$, which will be used to split sampling points in a ray into static points and dynamic points. We evaluate the effectiveness of this inference method in the test views and find that the recall and precision are reasonable for splitting the dynamic and static parts (recall: 0.97, precision: 0.94 when $\beta = 0.9$). Although the recall seems sufficient to retrieve most dynamic parts, we empirically find some false negatives in the rendering images affect the rendering quality. To address this problem, we use a ray-wise max-pooling operation to identify the points near to a dynamic point as dynamic. The kernel size of max-pooling is set to $k_m = 21$, and the stride is set to 1. In this way, the recall is very closed to 1. Although many hyper-parameters are incorporated, we have empirically found that the thresholds γ and β are not sensitive over a wide range of reasonable values.

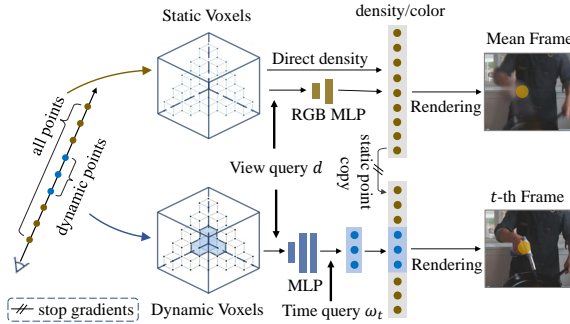


Figure 3. Illustration of our method. Given a ray, we first sample many points, and split them into static and dynamic ones using the variation field. After that, we pass all points to the static model to retrieve the density or color of all points, and render them to recover the mean pixel value. For the dynamic branch, we only pass the dynamic points and retrieve the density and color at a specific time step t (by the corresponding time query). Then we copy the values of static points from the static branch to render the pixel at time step t . Please note that each branch actually contains two voxel-grid representations to represent density and color respectively, while we only draw one for each branch here for simplicity.

3.4. Mixed Neural Voxels

With the help of the variation field, we can split a scene into dynamic voxels and static voxels. To reduce redundant computations, we use the lightweight static model described in Sec 3.1 to compute the densities and colors for static voxels and the dynamic model described in 3.2 to compute the densities and colors for dynamic voxels. The overall architecture is illustrated in Fig 3.

Specifically for a given ray $\mathbf{r}(s) = \mathbf{o} + s\mathbf{d}$ with origin \mathbf{o} and view direction \mathbf{d} , we apply stratified sampling from the near to the far planes and get N_s points. Then the N_s points are separated into static and dynamic ones by inferring these points with the proposed variation field. For the static branch, we pass all points to the static models and retrieve the colors and densities for each point to render the **mean pixel color** over time $\bar{\mathbf{C}}(\mathbf{r})$. For rendering, we use the volumetric rendering function [22, 24]:

$$\hat{\mathbf{C}}(\mathbf{r}) = \sum_{i=1}^{N_s} T_i \cdot (1 - \exp(-\bar{\sigma}_i \delta_i)) \cdot \bar{\mathbf{c}}_i \quad (6)$$

where T_i is the accumulated opacity which is formulated as: $T_i = \exp(-\sum_{j=1}^{i-1} \sigma_j \delta_j)$, and δ_i is the distance between adjacent samples. An l_2 -loss is employed to train the static model:

$$\underset{\mathcal{S}, \theta}{\text{minimize}} \mathcal{L}_s(\mathbf{r}) = \|\hat{\mathbf{C}}(\mathbf{r}) - \bar{\mathbf{C}}(\mathbf{r})\|_2^2 \quad (7)$$

For the dynamic branch, we use the model described in Sec 3.2 but only query the dynamic points to reduce most of the computation. Concretely, when the ray $\mathbf{r}(s)$ passes through at least one dynamic point, we calculate the density and color of these dynamic points at time step t through dynamic model \mathcal{G} . For the densities and colors of other static points in the ray, we copied them from the static output, which is equivalent to querying the density and color of these static points by the static model \mathcal{S} . Note that the copy operation is not back-propagated (with a detach operation) to avoid the dynamic supervision affecting the static branch. Formally, for the dynamic branch, we merge the static points and dynamic points to the final mixed representation $\dot{\sigma}, \dot{\mathbf{c}}$:

$$\dot{\sigma}(\mathbf{x}, t), \dot{\mathbf{c}}(\mathbf{x}, \mathbf{d}, t) = \begin{cases} \sigma(\mathbf{x}, t), \mathbf{c}(\mathbf{x}, \mathbf{d}, t) & \dot{\mathbf{M}}_{\mathbf{x}} = 1 \\ \text{st}(\bar{\sigma}(\mathbf{x})), \text{st}(\bar{\mathbf{c}}(\mathbf{x}, \mathbf{d})) & \dot{\mathbf{M}}_{\mathbf{x}} = 0 \end{cases}$$

where $\mathbf{x} := (x, y, z)$ represents the 3D position for simplicity and st represents the stop-gradients operation.

With $\dot{\sigma}$ and $\dot{\mathbf{c}}$, we use volumetric rendering to render the corresponding pixel color. Similarly, we calculate the rendered color $\hat{\mathbf{C}}^{(t)}(\mathbf{r})$ at time step t with the volumetric render function in Eq 6. The loss function is:

$$\underset{\mathcal{G}, \theta_{[1,2]}, \omega^{[\sigma, \mathbf{c}]}}{\text{minimize}} \mathcal{L}_d(\mathbf{r}) = \frac{1}{N_t} \sum_{t=1}^{N_t} \|\hat{\mathbf{C}}^{(t)}(\mathbf{r}) - \mathbf{C}^{(t)}(\mathbf{r})\|_2^2 \quad (8)$$

The overall loss is $\mathcal{L}(\mathbf{r}) = \mathcal{L}_s(\mathbf{r}) + \mathcal{L}_d(\mathbf{r})$. For both static and dynamic branches, we omit the computation of color for points whose densities are close to zero, which is a widely adopted pruning strategy [6, 19, 49].

Efficiency analysis: We define the proportion of dynamic points in a scene as λ (≈ 0.05 for most scenes). Besides, the FLOPs of static and dynamic branches are denoted as FLOP_{sta} and FLOP_{dyn} , respectively. Then the total FLOPs of MixVoxels are $\text{FLOP}_{\text{sta}} + \lambda \cdot \text{FLOP}_{\text{dyn}}$. Empirically, $\text{FLOP}_{\text{dyn}} / \text{FLOP}_{\text{sta}}$ ranges from 50 to 100 with different reasonable dimension settings. Then the acceleration ratio of splitting static and dynamic models is $\text{FLOP}_{\text{dyn}} / (\text{FLOP}_{\text{sta}} + \lambda \cdot \text{FLOP}_{\text{dyn}}) \approx 10$. In practice, the actual speedup with a 3090 GPU is about 5, the inconsistency between analysis and experiment may come from the GPU features, which are friendly to a more consistent network.

3.5. Implementation Detail

The voxel-grid representations require large GPU memory to store the cubically growing voxel numbers. To implement the voxel-grid representations more memory efficient, we use the tensor factorization technique proposed in TensorRF [6] to reduce the memory footprint. In this way, a 3D tensor is factorized into the outer product of a vector and a 2D matrix. We factorize all the voxel-grid tensors, including static voxels, dynamic voxels and the variation field. With the help of tensor factorization, the learned model costs about 500MB for a 300-frame multi-view video scene. For the voxel resolutions, we follow [6] to start from an initial low resolution of 256^3 , and upsample the resolution at steps 1500, 2000, 2500, and 2750 with a linear increase in the log space. The final resolution is set to 640^3 . Once the resolution is changed, we re-train the variation field, which only takes about 15-30s. The voxel-grid feature dimension is set to 27, and the hidden state of MLP is set to 512. For training, we use Adam [12] optimizer with a learning rate of 0.02 for voxels and $3e-3$ for MLPs. The total variation loss [49] is incorporated as a regularization to encourage the space smoothness.

4. Experiments

4.1. Experiment Setting

Dataset: We validate our method on the Plenoptic Video Dataset [16], which consists of 6 publicly accessible scenes: coffee-martini, flame-salmon, cook-spinach, cut-roasted-beef, flame-steak, sear-steak. We conduct experiments on all six datasets. Each scene contains 19 videos with different camera views. The dataset contains many challenging scenes including objects with topology changes, objects with volumetric effects, various lighting conditions, etc. For training and evaluation, we follow the experiment setting in [16] that employs 18 views for training and 1 view for

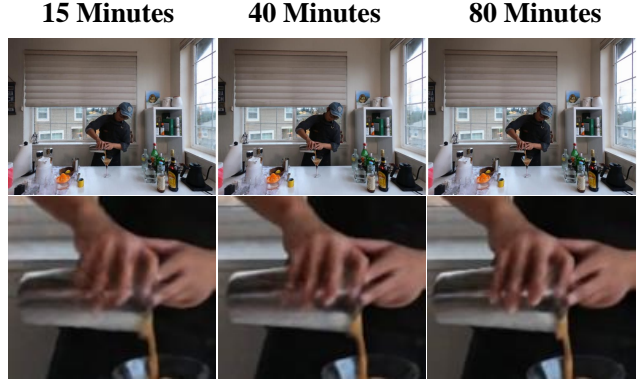


Figure 4. Qualitative demonstration of different training schedules. The three column represent training with 15, 40 and 80 minutes. Longer training helps reconstruct the highly-dynamic parts. The waving hand is zoomed in for a better observation.

evaluation. The videos are captured by GoPro Black Hero7 cameras at a resolution of 2028×2704 and frame rate of 30 FPS. The camera intrinsic and extrinsic parameters are estimated by COLMAP [33].

Evaluation Metrics: To quantitatively evaluate the rendering quality on novel views, we employ the following metrics as measurements: (1) Peak signal-to-noise ratio (PSNR); (2) Structural dissimilarity index measure (DSSIM); (3) Perceptual quality measure LPIPS [52]; (4) Perceived error difference FLIP [1]; (5) Just-Objectable-Difference (JOD) [13]. We follow the setting of [16] to evaluate our model frame by frame. For videos consisting of equal or more than 300 frames, we evaluate our model every 10 frames [16] to calculate the frame-by-frame metrics except for the JOD metrics, which requires a stack of continuous video.

Training Schedules: To evaluate the effect of different training time, we train MixVoxels with different schedules:

Model	Iterations	Training Time
MixVoxels-T	5000	15 min
MixVoxels-S	7500	25 min
MixVoxels-M	12500	40 min
MixVoxels-L	25000	80 min

Table 1. Models trained with different iterations.

4.2. Training and Rendering Efficiency

We compared the training efficiency of MixVoxels with previous state-of-the-art methods, shown in Table 2. For a dynamic scene with 300-frame multi-view videos, we reduce the training time from 1.3K GPU hours to 0.25 GPU hours (with a $5000 \times$ speedup), making the training of complex dynamic scenes more practical. Compared with concurrent works streaming radiance field [15] and NeRF-Player [36], MixVoxels achieves better results with only 15 minutes of training. For rendering, the MixVoxels has a

Method	Train	Render FPS	Size	PSNR
DyNeRF [16]	7 days *	–	28 MB	29.58
Stream [15]	75 min	8.3	5310MB	28.26
NeRFPlayer [36]	360 min	0.045	–	30.69
MixVoxels-T	15 min	16.7	500 MB	30.71
MixVoxels-S	25 min	16.7	500 MB	30.79
MixVoxels-M	40 min	16.7	500 MB	30.79
MixVoxels-L	80 min	16.7	500 MB	30.80

Table 2. Training and rendering efficiency comparisons for different methods. All metrics are measured on 300-frame scenes. The training time are copied from the original papers. * DyNeRF is trained on 8 GPUs, others are trained with one GPU.

17.6 fps rendering speed for 1K resolution and 65.4 fps for 0.5K resolution. For the model size, our model requires about 500MB of memory which is large than the implicit neural volumetric method DyNeRF. This is inevitable due to the cubically growing voxel numbers. However, compared with other voxel-grid based methods, our model is more compact because we take advantage of the tensor factorization proposed in TensorRF [6], which reduces the space complexity from $\mathcal{O}(n^3)$ to $\mathcal{O}(n^2)$.

Effect of training time: We study the effect of different training time. From the bottom part of Tab 2 and 3, we observe that most metrics are improved with a longer training. The bonus from training longer time diminishes when the training time exceeds 80 minutes. Fig 4 demonstrates the qualitative comparison. With 15 minutes of training, most components of the scene are recovered well enough, while the motion details are blurry. With longer training, the waving hand becomes clearer with a distinct boundary. Although most metrics of training 80 minutes are slightly better than training 40 minutes, we found that the differences are small in human perception. Training 40 minutes is enough for most scenes.

4.3. Rendering Quality Evaluation

Fig 1 and Fig 5 demonstrate the novel view rendering results on different dynamic scenes. We directly train our models on 10 seconds of 30-FPS videos for 25K iterations. The results show that our method can achieve near photo-realistic rendering quality. We provide the video results at our [project website](#). For quantitative results, we measure the representative metrics for each dynamic scene in the plenoptic video dataset, and the results are shown in Tab 4. We also compare our method with previous performant methods, shown in Tab 3. The comparison shows that MixVoxels achieves competitive performances compared with previous state-of-the-art method, while MixVoxels requires only 1/5000 to 1/1000 training time.

4.4. Ablation Study

In this subsection, we empirically justify the design of MixVoxels by ablating or modifying several key features.

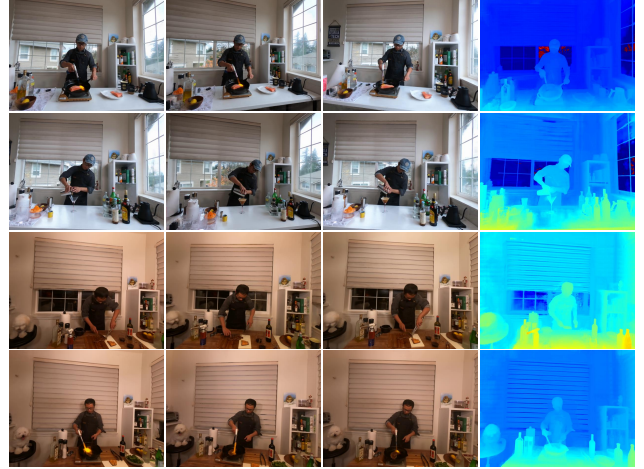


Figure 5. Novel view synthesis of MixVoxels. We select several frames with different views and time steps. The last column demonstrates the normalized depth in color space. For the whole video, we provide them at the [project website](#).

Method	PSNR↑	DSSIM↓	LPIPS↓	FLIP↓	JOD↑
MVS	19.1213	0.1116	0.2599	0.2542	-
NV	22.7975	0.0618	0.2951	0.2049	6.50
LLFF	23.2388	0.0762	0.2346	0.1867	6.48
NeRF-T	28.4487	0.0228	<u>0.1000</u>	0.1415	7.73
DyNeRF	<u>29.5808</u>	0.0197	0.0832	<u>0.1347</u>	8.07
MixVoxels-T	30.7101	0.0237	0.1617	0.1271	7.81
MixVoxels-S	30.7909	0.0219	0.1466	0.1272	7.88
MixVoxels-M	30.7872	0.0208	0.1356	0.1269	7.91
MixVoxels-L	30.8040	<u>0.0199</u>	0.1261	0.1282	<u>7.94</u>

Table 3. Quantitative comparison of different methods. The **best** and second best are marked. [15] and [36] only provide the PSNR results, we compare with them in Tab 2.

Dataset	PSNR↑	DSSIM↓	LPIPS↓	FLIP↓	JOD↑
Spinch	31.6097	0.0175	0.1162	0.1356	7.8518
Coffe	29.3584	0.0271	0.1492	0.1105	7.7427
Salmon	29.9163	0.0277	0.1592	0.1088	7.7840
Beef	31.3004	0.0174	0.1146	0.1360	7.9565
Sear	31.2082	0.0145	0.1074	0.1425	8.1288
Flame	31.4310	0.0152	0.1101	0.1359	8.1835
Mean	30.8040	0.0199	0.1261	0.1282	7.9412

Table 4. Quantitative results on six different dynamic scenes [16]. We report the average performances in the last row.

We also provide analysis that intuitively explains the ablations. We conduct all experiments in this subsection on the coffee-martini scene, which we find is typical for demonstrating the fast-moving complex objects.

Ablation on splitting voxels. To study the effect of splitting static and dynamic voxels, we compare MixVoxels with a full-dynamic voxel-grid representation, which all points are processed by the dynamic model. Tab 5 shows the comparisons. With the same training iterations, the full-dynamic model is more time-consuming, which is intuitive



Figure 6. Qualitative comparison of MixVoxels and the full-dynamic model. Training with full-dynamic models with the same iterations can not learn the dynamics well.

Method	Time	PSNR \uparrow	DSSIM \downarrow	LPIPS \downarrow	FLIP \downarrow	JOD \uparrow
Full-Dynamic	2.5h	28.36	0.036	0.2236	0.1196	7.44
MixVoxels	0.6h	29.00	0.029	0.1644	0.1167	7.64

Table 5. Ablation on the mixed voxels. Training with the full-dynamic voxel model hurts both efficiency and efficacy.

Method	Time	PSNR \uparrow	DSSIM \downarrow	LPIPS \downarrow	FLIP \downarrow	JOD \uparrow
Concat	58m	28.95	0.037	0.2146	0.1294	7.44
Fourier	43m	28.67	0.029	0.1824	0.1286	7.60
Inner-product	40m	29.00	0.029	0.1644	0.1167	7.64

Table 6. Ablation on three different methods for time query. We only substitute the time query with different method, and train them on the proposed MixVoxels framework.

because it processes all voxels with the dynamic models. Besides, the full-dynamic model achieves sub-optimal performance. Fig 6 shows the qualitative comparison. The full-dynamic model recovered blurred motions. We speculate the reason is because the large area of static regions affects the capturing of dynamic information. The network will be biased by most static voxels with no motions and tend to learn low-frequency information.

Ablation on time query: We compare our inner-product time query method with other variants: (1) Concatenation which concatenates the temporal embedding with the voxel features to be processed by an MLP. (2) Fourier head proposed by [46] which reconstructs the dynamics in frequency-domain. Tab 6 shows the performance comparison. The concatenation query method is both space- and time-consuming. Querying one time step requires forwarding the fused features through the whole MLP. Limited by the GPU memory, we can only query 50 time steps per-iteration with the concatenation way, which harms the performance on high-dynamic regions. The Fourier head processes the features to predict the magnitudes of different frequency components and the performance is competitive, while it requires an additional inverse discrete Fourier transform to recover the information in the temporal domain. Overall, the inner-product query is the simplest and most efficient way for querying.

Number of time queries per-iteration: We empirically

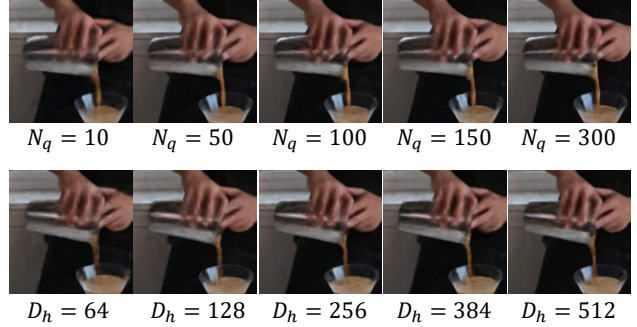


Figure 7. The first row demonstrates qualitative results of setting five different numbers of time query. The second row demonstrates the results of setting five different hidden dimensions.

find that simultaneously querying many different time steps in an iteration helps reconstruct the details of moving objects. The first row of Fig 7 demonstrates the effect of different numbers of time queries N_q . With more time queries, the boundaries of the moving hand and the flowing coffee become clearer. Querying more time steps can provide dense supervision and make the model acquire global temporal information in every iteration, which accelerates the convergence speed. The effective inner-product time queries allow adding more time queries with negligible increase in computation.

Ablations on MLPs: The choice of hidden dimensions in MLPs in the dynamic branch is also important to recover highly-dynamic components. The two dynamic MLPs for density and color have the same architecture which consists of three layers inserted by the activation layer, the dimension of hidden layer is denoted as D_h . We study the effect of D_h by setting different dimensions. The second row of Fig 7 demonstrates the qualitative results. Models with more hidden dimensions recover the moving hand sharper. We intuitively speculate that networks with larger hidden dimensions have greater capacity to better decompress the compact features stored in each voxel.

4.5. Limitations



Our method can synthesize novel view videos with near photo-realistic qualities for most scenes. However, for some scenes with complex lighting conditions, some artifacts appear at the boundary between dynamic and static voxels. The above figure shows the situation. The left group are recovered well. But in some views like the right group, artifacts emerge at the positions around the head. We suspect that the phenomenon is caused by the under-sampling of dynamic regions on scenes with some bad conditions. We will

investigate ways to address the problem in future works.

5. Conclusion

This paper demonstrates a new method named MixVoxels to efficiently reconstruct the 4D dynamic scenes and synthesize novel view videos. The core of our method is to split the 3D space into static and dynamic components with the proposed variation field, and process them with different branches. The separation speeds up the training and makes the dynamic branch focus on the dynamic parts to improve the performance. We also design an efficient dynamic voxel-grid representation with an inner-product time query. The proposed method achieves competitive results with only 15 minutes of training, making the training and rendering of complex dynamic scenes more practical. We believe the fast training speed will enable potentially useful applications that are bottlenecked by training efficiency.

References

- [1] Pontus Andersson, Jim Nilsson, Tomas Akenine-Möller, Magnus Oskarsson, Kalle Åström, and Mark D Fairchild. Flip: A difference evaluator for alternating images. *Proc. ACM Comput. Graph. Interact. Tech.*, 3(2):15–1, 2020.
- [2] Aayush Bansal, Minh Vo, Yaser Sheikh, Deva Ramanan, and Srinivasa Narasimhan. 4d visualization of dynamic events from unconstrained multi-view videos. In *Proceedings of the IEEE/CVF Conference on Computer Vision and Pattern Recognition*, pages 5366–5375, 2020.
- [3] Jonathan T Barron, Ben Mildenhall, Matthew Tancik, Peter Hedman, Ricardo Martin-Brualla, and Pratul P Srinivasan. Mip-nerf: A multiscale representation for anti-aliasing neural radiance fields. In *Proceedings of the IEEE/CVF International Conference on Computer Vision*, pages 5855–5864, 2021.
- [4] Jonathan T Barron, Ben Mildenhall, Dor Verbin, Pratul P Srinivasan, and Peter Hedman. Mip-nerf 360: Unbounded anti-aliased neural radiance fields. In *Proceedings of the IEEE/CVF Conference on Computer Vision and Pattern Recognition*, pages 5470–5479, 2022.
- [5] Chris Buehler, Michael Bosse, Leonard McMillan, Steven Gortler, and Michael Cohen. Unstructured lumigraph rendering. In *Proceedings of the 28th annual conference on Computer graphics and interactive techniques*, pages 425–432, 2001.
- [6] Anpei Chen, Zexiang Xu, Andreas Geiger, Jingyi Yu, and Hao Su. Tensorf: Tensorial radiance fields. *arXiv preprint arXiv:2203.09517*, 2022.
- [7] Paul E Debevec, Camillo J Taylor, and Jitendra Malik. Modeling and rendering architecture from photographs: A hybrid geometry-and image-based approach. In *Proceedings of the 23rd annual conference on Computer graphics and interactive techniques*, pages 11–20, 1996.
- [8] Yilun Du, Yinan Zhang, Hong-Xing Yu, Joshua B Tenenbaum, and Jiajun Wu. Neural radiance flow for 4d view synthesis and video processing. In *2021 IEEE/CVF International Conference on Computer Vision (ICCV)*, pages 14304–14314. IEEE Computer Society, 2021.
- [9] John Flynn, Michael Broxton, Paul Debevec, Matthew Duvall, Graham Fyffe, Ryan Overbeck, Noah Snavely, and Richard Tucker. Deepview: View synthesis with learned gradient descent. In *Proceedings of the IEEE/CVF Conference on Computer Vision and Pattern Recognition*, pages 2367–2376, 2019.
- [10] Chen Gao, Ayush Saraf, Johannes Kopf, and Jia-Bin Huang. Dynamic view synthesis from dynamic monocular video. In *Proceedings of the IEEE/CVF International Conference on Computer Vision*, pages 5712–5721, 2021.
- [11] Takeo Kanade, Peter Rander, and PJ Narayanan. Virtualized reality: Constructing virtual worlds from real scenes. *IEEE multimedia*, 4(1):34–47, 1997.
- [12] Diederik P Kingma and Jimmy Ba. Adam: A method for stochastic optimization. *arXiv preprint arXiv:1412.6980*, 2014.
- [13] Vamsi Kiran Adhikarla, Marek Vinkler, Denis Sumin, Rafal K Mantiuk, Karol Myszkowski, Hans-Peter Seidel, and Piotr Didyk. Towards a quality metric for dense light fields. In *Proceedings of the IEEE Conference on Computer Vision and Pattern Recognition*, pages 58–67, 2017.
- [14] Kiriakos N Kutulakos and Steven M Seitz. A theory of shape by space carving. *International journal of computer vision*, 38(3):199–218, 2000.
- [15] Lingzhi Li, Zhen Shen, Zhongshu Wang, Li Shen, and Ping Tan. Streaming radiance fields for 3d video synthesis. *arXiv preprint arXiv:2210.14831*, 2022.
- [16] Tianye Li, Mira Slavcheva, Michael Zollhoefer, Simon Green, Christoph Lassner, Changil Kim, Tanner Schmidt, Steven Lovegrove, Michael Goesele, Richard Newcombe, et al. Neural 3d video synthesis from multi-view video. In *Proceedings of the IEEE/CVF Conference on Computer Vision and Pattern Recognition*, pages 5521–5531, 2022.
- [17] Zhengqi Li, Simon Niklaus, Noah Snavely, and Oliver Wang. Neural scene flow fields for space-time view synthesis of dynamic scenes. In *Proceedings of the IEEE/CVF Conference on Computer Vision and Pattern Recognition*, pages 6498–6508, 2021.
- [18] David B Lindell, Julien NP Martel, and Gordon Wetzstein. Autoint: Automatic integration for fast neural volume rendering. In *Proceedings of the IEEE/CVF Conference on Computer Vision and Pattern Recognition*, pages 14556–14565, 2021.
- [19] Lingjie Liu, Jiatao Gu, Kyaw Zaw Lin, Tat-Seng Chua, and Christian Theobalt. Neural sparse voxel fields. *Advances in Neural Information Processing Systems*, 33:15651–15663, 2020.
- [20] Stephen Lombardi, Tomas Simon, Jason Saragih, Gabriel Schwartz, Andreas Lehrmann, and Yaser Sheikh. Neural volumes: Learning dynamic renderable volumes from images. *arXiv preprint arXiv:1906.07751*, 2019.
- [21] Ricardo Martin-Brualla, Noha Radwan, Mehdi SM Sajjadi, Jonathan T Barron, Alexey Dosovitskiy, and Daniel Duckworth. Nerf in the wild: Neural radiance fields for unconstrained photo collections. In *Proceedings of the IEEE/CVF*

- Conference on Computer Vision and Pattern Recognition*, pages 7210–7219, 2021.
- [22] Nelson Max. Optical models for direct volume rendering. *IEEE Transactions on Visualization and Computer Graphics*, 1(2):99–108, 1995.
 - [23] Ben Mildenhall, Pratul P Srinivasan, Rodrigo Ortiz-Cayon, Nima Khademi Kalantari, Ravi Ramamoorthi, Ren Ng, and Abhishek Kar. Local light field fusion: Practical view synthesis with prescriptive sampling guidelines. *ACM Transactions on Graphics (TOG)*, 38(4):1–14, 2019.
 - [24] Ben Mildenhall, Pratul P Srinivasan, Matthew Tancik, Jonathan T Barron, Ravi Ramamoorthi, and Ren Ng. Nerf: Representing scenes as neural radiance fields for view synthesis. *Communications of the ACM*, 65(1):99–106, 2021.
 - [25] Thomas Müller, Alex Evans, Christoph Schied, and Alexander Keller. Instant neural graphics primitives with a multiresolution hash encoding. *arXiv preprint arXiv:2201.05989*, 2022.
 - [26] Keunhong Park, Utkarsh Sinha, Jonathan T Barron, Sofien Bouaziz, Dan B Goldman, Steven M Seitz, and Ricardo Martin-Brualla. Nerfies: Deformable neural radiance fields. In *Proceedings of the IEEE/CVF International Conference on Computer Vision*, pages 5865–5874, 2021.
 - [27] Keunhong Park, Utkarsh Sinha, Peter Hedman, Jonathan T Barron, Sofien Bouaziz, Dan B Goldman, Ricardo Martin-Brualla, and Steven M Seitz. Hypernerf: A higher-dimensional representation for topologically varying neural radiance fields. *arXiv preprint arXiv:2106.13228*, 2021.
 - [28] Eric Penner and Li Zhang. Soft 3d reconstruction for view synthesis. *ACM Transactions on Graphics (TOG)*, 36(6):1–11, 2017.
 - [29] Albert Pumarola, Enric Corona, Gerard Pons-Moll, and Francesc Moreno-Noguer. D-nerf: Neural radiance fields for dynamic scenes. In *Proceedings of the IEEE/CVF Conference on Computer Vision and Pattern Recognition*, pages 10318–10327, 2021.
 - [30] Daniel Rebain, Wei Jiang, Soroosh Yazdani, Ke Li, Kwang Moo Yi, and Andrea Tagliasacchi. Derf: Decomposed radiance fields. In *Proceedings of the IEEE/CVF Conference on Computer Vision and Pattern Recognition*, pages 14153–14161, 2021.
 - [31] Christian Reiser, Songyou Peng, Yiyi Liao, and Andreas Geiger. Kilonerf: Speeding up neural radiance fields with thousands of tiny mlps. In *Proceedings of the IEEE/CVF International Conference on Computer Vision*, pages 14335–14345, 2021.
 - [32] Gernot Riegler and Vladlen Koltun. Free view synthesis. In *European Conference on Computer Vision*, pages 623–640. Springer, 2020.
 - [33] Johannes L Schonberger and Jan-Michael Frahm. Structure-from-motion revisited. In *Proceedings of the IEEE conference on computer vision and pattern recognition*, pages 4104–4113, 2016.
 - [34] Steven M Seitz and Charles R Dyer. Photorealistic scene reconstruction by voxel coloring. *International Journal of Computer Vision*, 35(2):151–173, 1999.
 - [35] Vincent Sitzmann, Justus Thies, Felix Heide, Matthias Nießner, Gordon Wetzstein, and Michael Zollhofer. Deepvoxels: Learning persistent 3d feature embeddings. In *Proceedings of the IEEE/CVF Conference on Computer Vision and Pattern Recognition*, pages 2437–2446, 2019.
 - [36] Liangchen Song, Anpei Chen, Zhong Li, Zhang Chen, Lele Chen, Junsong Yuan, Yi Xu, and Andreas Geiger. Nerfplayer: A streamable dynamic scene representation with decomposed neural radiance fields. *arXiv preprint arXiv:2210.15947*, 2022.
 - [37] Pratul P Srinivasan, Ben Mildenhall, Matthew Tancik, Jonathan T Barron, Richard Tucker, and Noah Snavely. Lighthouse: Predicting lighting volumes for spatially-coherent illumination. In *Proceedings of the IEEE/CVF Conference on Computer Vision and Pattern Recognition*, pages 8080–8089, 2020.
 - [38] Pratul P Srinivasan, Richard Tucker, Jonathan T Barron, Ravi Ramamoorthi, Ren Ng, and Noah Snavely. Pushing the boundaries of view extrapolation with multiplane images. In *Proceedings of the IEEE/CVF Conference on Computer Vision and Pattern Recognition*, pages 175–184, 2019.
 - [39] Cheng Sun, Min Sun, and Hwann-Tzong Chen. Direct voxel grid optimization: Super-fast convergence for radiance fields reconstruction. In *Proceedings of the IEEE/CVF Conference on Computer Vision and Pattern Recognition*, pages 5459–5469, 2022.
 - [40] Matthew Tancik, Vincent Casser, Xincheng Yan, Sabeek Pradhan, Ben Mildenhall, Pratul P Srinivasan, Jonathan T Barron, and Henrik Kretschmar. Block-nerf: Scalable large scene neural view synthesis. In *Proceedings of the IEEE/CVF Conference on Computer Vision and Pattern Recognition*, pages 8248–8258, 2022.
 - [41] Matthew Tancik, Pratul P Srinivasan, Ben Mildenhall, Sara Fridovich-Keil, Nithin Raghavan, Utkarsh Singhal, Ravi Ramamoorthi, Jonathan Barron, and Ren Ng. Fourier features let networks learn high frequency functions in low dimensional domains. *Advances in Neural Information Processing Systems*, 33:7537–7547, 2020.
 - [42] Justus Thies, Michael Zollhöfer, and Matthias Nießner. Deferred neural rendering: Image synthesis using neural textures. *ACM Transactions on Graphics (TOG)*, 38(4):1–12, 2019.
 - [43] Edgar Tretschk, Ayush Tewari, Vladislav Golyanik, Michael Zollhöfer, Christoph Lassner, and Christian Theobalt. Non-rigid neural radiance fields: Reconstruction and novel view synthesis of a dynamic scene from monocular video. In *Proceedings of the IEEE/CVF International Conference on Computer Vision*, pages 12959–12970, 2021.
 - [44] Richard Tucker and Noah Snavely. Single-view view synthesis with multiplane images. In *Proceedings of the IEEE/CVF Conference on Computer Vision and Pattern Recognition*, pages 551–560, 2020.
 - [45] Michael Waechter, Nils Moehrle, and Michael Goesele. Let there be color! large-scale texturing of 3d reconstructions. In *European conference on computer vision*, pages 836–850. Springer, 2014.
 - [46] Liao Wang, Jiakai Zhang, Xinhang Liu, Fuqiang Zhao, Yanshun Zhang, Yingliang Zhang, Minye Wu, Jingyi Yu, and

- Lan Xu. Fourier plenotrees for dynamic radiance field rendering in real-time. In *Proceedings of the IEEE/CVF Conference on Computer Vision and Pattern Recognition*, pages 13524–13534, 2022.
- [47] Daniel N Wood, Daniel I Azuma, Ken Aldinger, Brian Curless, Tom Duchamp, David H Salesin, and Werner Stuetzle. Surface light fields for 3d photography. In *Proceedings of the 27th annual conference on Computer graphics and interactive techniques*, pages 287–296, 2000.
- [48] Wenqi Xian, Jia-Bin Huang, Johannes Kopf, and Changil Kim. Space-time neural irradiance fields for free-viewpoint video. In *Proceedings of the IEEE/CVF Conference on Computer Vision and Pattern Recognition*, pages 9421–9431, 2021.
- [49] Alex Yu, Sara Fridovich-Keil, Matthew Tancik, Qinhong Chen, Benjamin Recht, and Angjoo Kanazawa. Plenoxels: Radiance fields without neural networks. *arXiv preprint arXiv:2112.05131*, 2021.
- [50] Alex Yu, Ruilong Li, Matthew Tancik, Hao Li, Ren Ng, and Angjoo Kanazawa. Plenotrees for real-time rendering of neural radiance fields. In *Proceedings of the IEEE/CVF International Conference on Computer Vision*, pages 5752–5761, 2021.
- [51] Kai Zhang, Gernot Riegler, Noah Snavely, and Vladlen Koltun. Nerf++: Analyzing and improving neural radiance fields. *arXiv preprint arXiv:2010.07492*, 2020.
- [52] Richard Zhang, Phillip Isola, Alexei A Efros, Eli Shechtman, and Oliver Wang. The unreasonable effectiveness of deep features as a perceptual metric. In *Proceedings of the IEEE conference on computer vision and pattern recognition*, pages 586–595, 2018.
- [53] Tinghui Zhou, Richard Tucker, John Flynn, Graham Fyffe, and Noah Snavely. Stereo magnification: Learning view synthesis using multiplane images. *arXiv preprint arXiv:1805.09817*, 2018.
- [54] C Lawrence Zitnick, Sing Bing Kang, Matthew Uyttendaele, Simon Winder, and Richard Szeliski. High-quality video view interpolation using a layered representation. *ACM transactions on graphics (TOG)*, 23(3):600–608, 2004.